RADIO SCIENCE, VOL. 41, RS4002, doi:10.1029/2005RS003371, 2006

An interhemispheric model of artificial ionospheric ducts

R. P. Perrine,[1] G. M. Milikh,[1] K. Papadopoulos,[1] J. D. Huba,[2] G. Joyce,[3] M. Swisdak,[3] and Y. Dimant[4]

Received 8 September 2005; revised 15 March 2006; accepted 23 March 2006; published 12 July 2006.

[1] A duct in Earth's ionosphere is characterized by density gradients perpendicular to the magnetic field, which enhance refractive indices and act as waveguides to whistler-range waves. Interhemispheric ducts along magnetic field lines have implications for the transmission of ELF radio waves across the globe. Strong HF ionospheric heating has been shown to create a depletion of electrons at the heated region and could lead to a pressure perturbation that propagates along the entire magnetic field line, potentially forming an artificial duct. Here we present results from an ionospheric numerical model used to study the effects of localized HF heating on an interhemispheric magnetic flux tube. The existing Sami2 is Another Model of the Ionosphere (SAMI2) ionospheric model has been modified to include a flexible source of strong HF heating that can be varied to mimic the fluctuations in HF heating efficiencies and ionospheric conditions. Our parametric study includes varying the heating source intensity and location along the magnetic field line, revealing both linear and nonlinear relationships connecting these source parameters to maximum pressure, temperature, and density perturbations; propagation velocity of density perturbations; and characteristic heating and cooling times of the irradiated region. After a transient state, the duct structure achieves a quasi-steady state, showing electron depletion at the heated region and density enhancements in the regions just below and above the heated region. The density perturbations propagate deep inside the plasmasphere to the conjugate F_2 peak, with density enhancements along the traveling pulse boundary. The possibility of generating interhemispheric ducts is discussed.

Citation: Perrine, R. P., G. M. Milikh, K. Papadopoulos, J. D. Huba, G. Joyce, M. Swisdak, and Y. Dimant (2006), An interhemispheric model of artificial ionospheric ducts, *Radio Sci.*, *41*, RS4002, doi:10.1029/2005RS003371.

1. Introduction and Motivation

[2] Numerous observations show that strong electron heating in the ionosphere can be generated by powerful HF facilities such as HIPAS, EISCAT, and HAARP [see, e.g., *Ferraro et al.*, 1989; *Barr and Stubbe*, 1993; *Papadopoulos et al.*, 2003, 2005]. It has been observed that the electron heating is followed by expulsion of the plasma from the heated region, resulting in cavity formation [see *Duncan et al.*, 1988].

[3] It has been suggested that HF heating at the F_2 peak of the ionosphere could generate a strong pressure pulse in the dense plasma, confined to travel along the more rarefied magnetic field line. As shown in previous work by *Vas'kov et al.* [1992, 1993] and *Huba et al.* [2000b], the pressure pulse could propagate in the topside ionosphere and magnetosphere, expelling plasma as it travels, leading to the formation of magnetically field-aligned plasma density depletions. Those density depletions can serve as ducts for ELF waves, both of natural and artificial origin, in the following manner: the density gradient perpendicular to the magnetic field line causes an index of refraction gradient that can lead to total internal reflection of the ELF waves. If these density gradients are strong enough, and extend along the entirety of the field line, the ELF wave will continuously

[1]Department of Astronomy, University of Maryland, College Park, Maryland, USA.
[2]Plasma Physics Division, Naval Research Laboratory, Washington, DC, USA.
[3]Icarus Research, Inc., Bethesda, Maryland, USA.
[4]Center for Space Physics, Boston University, Boston, Massachusetts, USA.

0048-6604/06/2005RS003371$11.00

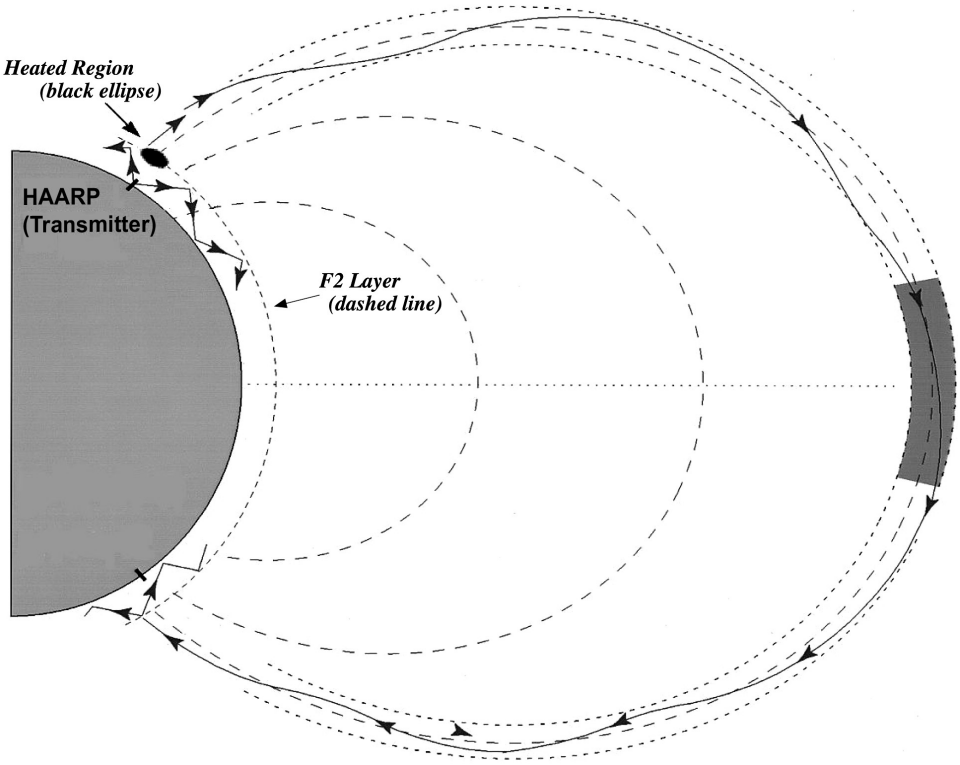

Figure 1. Cartoon of the Earth and an artificial ionospheric duct. After the heater perturbs the heated region, the density perturbation follows the magnetic field line to the opposite hemisphere. Once formed, the duct can be used to guide ELF radio waves to the opposite hemisphere as shown.

reflect off of the boundaries of the duct, and can be channeled from one endpoint of the field line to the other, as depicted in Figure 1. Hence the duct becomes a magnetically aligned waveguide, functioning under the same principle as a fiber optic cable, yet runs from one hemisphere of the Earth to the other.

[4] Natural ducts form in the ionosphere without any human intervention. *Helliwell* [1974] presented an initial theoretical model for how these natural ducts could be used, and later *Inan et al.* [2004] successfully detected ELF transmissions while aboard a ship in the South Pacific, transmissions identical to those created by the HAARP transmitter in Gakona, Alaska. However, it will be important to create artificial ducts if the reliable interhemisphere transmission of whistler waves is to become feasible.

[5] The study of artificial duct formation observationally requires measuring the ionosphere at high temporal and spatial resolution (on the order of minutes and hundreds of kilometers). This is difficult to do with existing technology and equipment, as the spatial volume of the ionosphere is immense ($>10^6$ km^3). Low-resolution measurements can be made by satellites (the American DMSP cluster, and the French "Demeter" satellite) and Incoherent Scattering Radars. A future project called "Resonance" (see http://ilws.gsfc.nasa.gov/russia_cospar.pdf for preliminary details) is planned to perform sampling of the ionosphere along a magnetic field line which should provide excellent spatial resolution.

[6] In this paper, computer simulations are employed to study processes that could lead to field-aligned duct formation using strong HF ionospheric heating. It is the objective of this paper to demonstrate the plausibility of this principle by presenting results from a self-consistent global computational model of the ionosphere in the presence of strong thermal perturbations, like those from HF heating. This paper will also detail how the structure and formation of such a duct might be affected by variations in the heating parameters. The model used is a modified version of the ionospheric code SAMI2 [*Huba et al.*, 2000a]. Results suggest that density perturbations can extend across the entire magnetic field line, and even reach the conjugate F_2 peak, approximately 28,000 km from the heated region.

[7] The paper is organized as follows: Section 2 describes the details of the global computational model

used in this study. Section 3 presents the simulation procedure, as well as justifications for the conditions of our simulations, while results from these simulations are detailed in section 4. Finally, section 5 presents discussion and conclusions, with suggestions for future work in section 6.

2. SAMI2 Ionospheric Heating Model

[8] We use the ionospheric model SAMI2, developed at the Naval Research Laboratory [*Huba et al.*, 2000a], to conduct simulations with a realistic ionosphere. It is an Eulerian grid-based code, which considers an ionosphere made up of 7 ion species: H^+, He^+, O^+, O_2^+, N^+, N_2^+, and NO^+. The equations of continuity and momentum are solved for each ion species, with the temperature equation solved for the electrons and the ion species H^+, He^+, and O^+. Electron density is determined by summing the densities of each ion species, as quasi-neutrality is assumed everywhere in the plasma, and parallel electron velocity (with respect to the ions) is assumed to be zero.

[9] The code includes an interhemispheric dipole field model, $\mathbf{E} \times \mathbf{B}$ drift of the field lines (in altitude and latitude), a neutral atmosphere model, horizontal winds, photodeposition into the ionosphere, ion chemistry, and ion inertia. The inclusion of ion inertia allows for the study of sound wave propagation in the plasma. To our knowledge, SAMI2 is the only comprehensive interhemispheric ionosphere code to include ion inertia, which is a critical feature for our work.

[10] Since the model is interhemispheric, SAMI2 can simulate the plasma along entire magnetic dipole field lines, from the topside magnetosphere down to nearly the *E* layer (approximately 85 km from the ground). Neutral species are set using two empirically measured models: the Mass Spectrometer Incoherent Scatter model (NRLMSIS00) [*Picone et al.*, 2002] and the Horizontal Wind Model (HWM93) [*Hedin et al.*, 1991].

[11] The version of SAMI2 used in this work was modified to include a localized flexible artificial heat source. In the original code, the electron temperature equation included heating terms from electron-neutral collisions, Q_{en}, electron-ion collisions, Q_{ei}, and photoelectron heating, Q_{phe}. A fourth electron heating term, Q_{HF}, representing artificial heating (i.e., that of a HF transmitter), has been added to the electron temperature equation in SAMI2:

$$\frac{\partial T_e}{\partial t} - \frac{2}{3}\frac{1}{n_e k} b_z^2 \frac{\partial}{\partial z}\kappa_e \frac{\partial T_e}{\partial z} = Q_{en} + Q_{ei} + Q_{phe} + Q_{HF} \tag{1}$$

The second term on the left side of the equation is a diffusion term, where κ_e is the parallel electron thermal conductivity, k the Boltzmann constant, and b_z the component of the magnetic field in the direction of the field line, normalized to its equatorial value on Earth's surface. *Huba et al.* [2000a] defines κ_e, Q_{en}, Q_{ei}, and Q_{phe} in detail.

[12] The Q_{HF} term is represented by a Gaussian-shaped source:

$$Q_{HF}(z) = q\, e^{-(z-z_0)^2/a^2} \tag{2}$$

$$q = \frac{\eta W}{V n_e k} \tag{3}$$

with $Q_{HF}(z)$ being the total heating rate per electron (in Kelvin per second) delivered to location z. The parameters of this term are the altitude of the heated spot's center z_0, the vertical extent of the heated region a, and the heating rate per electron q, which in turn is determined (in equation (3)) by the wave absorption coefficient η, the radiated HF power W, the HF heated volume V, the electron number density n_e, and Boltzmann's constant k.

[13] The heating parameters q, z_0, and a can be set directly in the SAMI2 code in order to explore a range of possible heater settings and atmospheric conditions. Encompassed in q are both the variations in the heater power W as well as the atmospheric electron density n_e.

[14] The height of the heated spot z_0 is in practice determined by the HF frequency of the heater, and the extent of the region a is determined by the plasma frequency of that altitude ω_e and the electron cyclotron frequency Ω_e. It has been shown that strong wave absorption occurs in a relatively thin region 10–20 km between the wave reflection point (where wave frequency ω equals the plasma frequency $\omega_e(z_0)$) and the location of the upper hybrid resonance (where $\omega = \sqrt{\omega_e(z_0 - a)^2 + \Omega_e^2}$). This region is filled with irregularities induced by the HF heating, and the wave scattering by those irregularities leads to the so-called "anomalous absorption" effect (as detailed by *Gurevich et al.* [1996]).

[15] The extent of the region a can be estimated by assuming that the electron density near the F_2 region of the ionosphere varies exponentially with height with a scale height of L. Once this density profile is assumed, the distance between the wave reflection point and the upper hybrid resonance is calculable (as in work by *Gurevich and Milikh* [1997, p. 391]) using $a = L\,(\Omega_e/\omega)^2$. Here ω is the frequency of the heater. This approximate equation is valid as long as a is small compared to L. For example, with L = 120 km, Ω_e = 1.4 MHz, and ω = 3.5–5 MHz, a is about 10–20 km.

[16] For the HAARP transmitter in Alaska, we've estimated that its current full-power production capabilities (960 kW) would produce a q of approximately 300 K/s. The projected facility (3.6 MW) will results

in a maximum q of roughly 5000 K/s. These values were obtained using equation (3) with typical values for the HAARP transmitter and from the SAMI2 simulation: the current maximum radiated power is about 936 kW at 4.5 MHz, with the two dimensions of antenna gain as 19.8° and 27.8°. The number density of electrons near the F_2 peak (in the SAMI2 code) is taken as 7×10^5 cm^{-3}. For simplicity, the absorption coefficient is assumed to be 0.6.

[17] The volume of the heated region is $V = \pi\, r_1\, r_2\, a$, where r_1 and r_2 are the horizontal dimensions of the heated region, resulting from antenna gain; a is the familiar vertical extent of the region, which can be taken as 10 km, as explained earlier.

[18] With these inputs, after making the necessary conversions, the value for q at a particular altitude and electron number density is

$$q = 3 \times 10^2 \frac{(380\ \text{km}/z_0)^2}{(n_e/7 \times 10^5\ \text{cm}^{-3})}\ \text{K/s} \qquad (4)$$

The coefficient is for the current HAARP capabilities. For the completed HAARP facility, the coefficient of 3×10^2 will be closer to 5×10^3, yielding greater than an order of magnitude increase in the energy delivered to each electron.

3. Simulation Setup and Procedure

[19] As our goal is to begin to understand duct formation and verify its basic plausibility, we used the SAMI2 model to study the plasma confined to a single magnetic field line. This is similar to performing a 1-D simulation, however SAMI2 incorporates 2-D effects, such as expansion of the field line at higher altitudes, which conserves magnetic flux. However, for simplicity, we ignore the $\mathbf{E} \times \mathbf{B}$ drift of the plasma, implicitly assuming that the plasma is perfectly confined to the field line. Thus this work examines the behavior of the plasma along a single field line embedded within a limited dynamic global environment. Further studies will have to be done to evaluate the validity of these simplifications.

[20] We varied two heating parameters during our parametric study of the plasma perturbations: the intensity of the HF source q and the altitude of the heated region z_0 (see equation (2)). The intensity range used is 100–5000 K/s; the lower end producing only slight perturbations in the ionosphere, and the higher end being the highest estimated intensity of which the completed HAARP facility will be capable.

[21] The heating altitude varied between 300–380 km. In these runs, the F_2 peak was located at about 380 km, as obtained from the SAMI2 nighttime model. Thus the lower end of our parameter space represents heating below the F_2 peak, while the higher end heats directly on the F_2 peak itself. In Figure 1, this is represented by placing the heated region (black ellipse) on the F_2 layer (dashed line circling Earth), or slightly below it. It is not physically possible to heat the ionosphere above the F_2 peak from the ground, so we did not study heating above this altitude. Our standard energy deposition width a (from equation (2)) was 20 km, extending below the F_2 peak.

[22] In reality, the electron density in the F_2 peak changes in time, under both natural and HF-heating conditions. Therefore, to keep the ionospheric absorption efficient one has to adjust the heating frequency to match it to the plasma frequency of the F_2 peak (which HAARP's design allows). This complication was not treated in the SAMI2 code, as our heating parameters z_0, q, and a are set by the user and are constant throughout the simulation. Future versions of the code will model these effects more closely, but our approach is a satisfactory approximation for this study.

[23] The chosen magnetic field line had its apex at 14,000 km (as measured from the ground along the field line), corresponding to a geographic latitude of approximately 54° [magnetic latitude of ~56°]. It should be mentioned that the version of SAMI2 used in this work is a midlatitude model, so we chose not to simulate the field lines above the HAARP site (latitude 62°N) in this study.

[24] Our simulations proceeded as follows. The code starts from its empirically measured initial conditions at 1000 LT (local time), and runs for 12 hours without any HF-heating perturbations. This practice allows the system to relax to ambient conditions, and reduces noise in the system due to the initial conditions. The sun sets at approximately 1900 LT in these runs, so the ionosphere cools and relaxes toward nighttime conditions during the end of this period. Then at 2200 LT, the "artificial heater" turns on and begins to pump energy into the electrons, using the specified parameters for that run. Artificial heating proceeds for 5 hours, continuously pumping energy into the electrons at the specified altitude, and the perturbations in ion and electron properties are tracked as they travel along the entire 1-D field line, to the opposite hemisphere. Then the heater switches off, allowing the ionosphere to relax back to ambient conditions. The simulation ends 2 hours later, just before the sun begins to rise. The total simulation time is 19 hours. 200 unequally spaced grid points were employed to obtain satisfactory resolution, with smaller grid spacing located at the lower altitudes in order to accurately study the denser regions. Results from trials with 2000 grid points did not differ significantly from our nominal grid choice. With 200 grid points, on a 2.20–3.40 GHz Pentium IV machine running Linux, a typical run took 1–3 hours of CPU time.

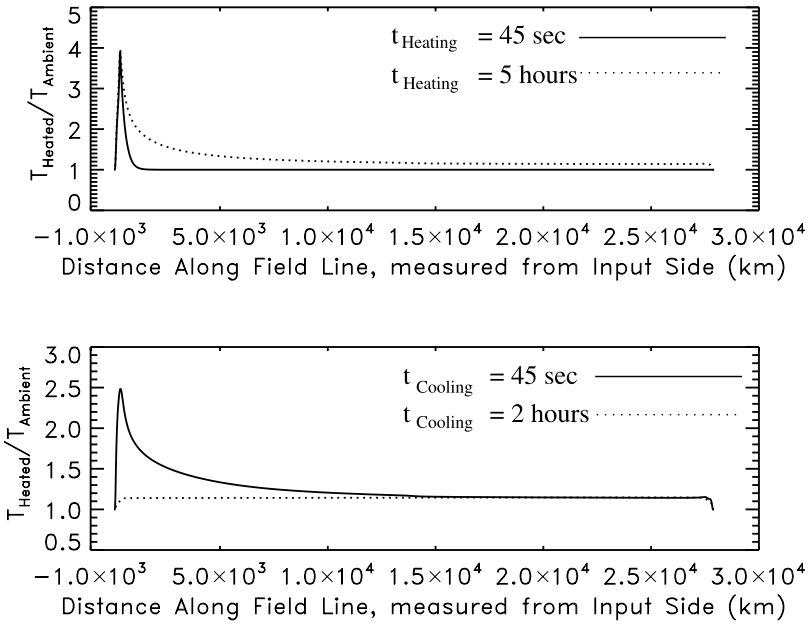

Figure 2. Electron temperature evolution during and after artificial heating. Normalized temperature perturbations are on the vertical axis, and the horizontal axis is the location on the field line, measured along the field line. In the top plot, the solid line corresponds to 45 s after heating begins, while the dotted line is 5 hours after heating begins. In the bottom plot, the solid line is 45 s after cooling begins, and the dotted line is after 2 hours of relaxation. Heating parameters for these data are q = 5000 K/s and z_0 = 380 km.

[25] In order to isolate and measure the perturbations directly, a duplicate set of runs are made with no artificial heating. For obvious reasons, we call this an "ambient" run, while those with artificial heating are "heated" runs. The ionosphere changes dramatically during a simulation because of unavoidable diurnal processes, and is never truly in equilibrium, so the perturbations in the heated runs due to artificial heating would not be easily discerned on their own. Yet since the same natural variations are present in the ambient data, scaling (or subtracting) by the ambient data provides a simple way to remove the noise and decouple the natural variations from the artificial perturbations.

4. Simulation Results

[26] The results of the simulations can be divided into two categories: general responses of the ionosphere to strong perturbations, and parametric responses to changes in heating parameters.

4.1. General Responses

[27] In each run, the heated region experienced a rapid increase in temperature upon the application of artificial heating. Then, in order to preserve pressure equilibrium, the region subsequently experienced a dramatic decrease in electron density. These perturbations did not remain local to the heated region, as can be seen in Figures 2 and 3. In them, electron temperature and density are normalized to their respective ambient values (i.e., the temperature at that location on the field line at that time, in the unheated data), and plotted versus location on the field line, so that values >1 indicate increases in that property during heating. It should be noted that the distances on the horizontal axis are as measured from the ground along the field line. The location of the heated region is at 380 km on these plots, on the F_2 peak.

[28] In the top plot of Figure 2, the solid line represents the temperature profile after only 45 s of artificial heating, displaying a large increase in temperature at the heated spot, yet little increase elsewhere. In the dotted line plotted over it, representing the system after 5 hours of heating, the temperature at the heated spot has not increased any further, but the temperature perturbation has spread to affect the entire system. This indicates that the temperature at the heated spot increases dramatically in a matter of seconds, but does not increase beyond that initial perturbation. Instead, the extra energy is carried away from that spot to increase the temperature everywhere in the system.

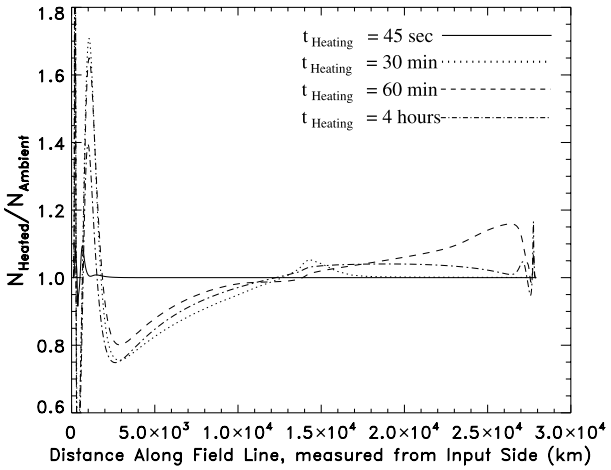

Figure 3. Density perturbation profile during artificial heating. Normalized density perturbations are on the vertical axis, and the horizontal axis is the location on the field line, measured along the field line. The solid line corresponds to 45 s after heating begins, the dotted line is 30 min after heating begins, the dashed line is 60 min after heating begins, and the dash-dotted line shows conditions after 4 hours of heating. Heating parameters for these data are q = 5000 K/s and z_0 = 380 km.

[29] The bottom plot in Figure 2 represents the system during cooling, when the artificial heater is turned off. It should be pointed out that the peak in the temperature seen in this line is not at the heated spot, but is some hundred kilometers away, and thus has not had time to cool. The overlaid dotted line represents the system at the end of the simulation, showing that the system rapidly returns to nearly ambient conditions after the removal of artificial heating.

[30] Figure 3 shows density profiles at various times during a typical simulation, showing how the perturbation in density moves through the system (toward the right on these plots). Since the lines nearly overlap on the left side of Figure 3, the side closer to the heater, it can be seen that the density perturbations that occur in response to heating are steady in the presence of steady heating. The solid line shows the system after 45 s of heating, and thus the perturbations have not yet grown in that region to their steady values. After 30 min, the system reaches the state shown by the dotted line; the hemisphere on the left has nearly reached its steady state, and the density perturbation is progressing to the right, passing the apex of the line. The dashed line, showing the system after 1 hour of heating, reveals the perturbation arriving at the conjugate region, close to the conjugate F_2 peak. In the final dash-dotted line, representing the system after 4 hours of heating, the steady state perturbations on the right side of the system mirror those on the left side, with smaller amplitudes. It is interesting to note that while the steady state of the heated region is a depletion of electrons, there are enhancements to the electron density above and below this heated spot, as though the electrons and ions were being displaced out of the heated region, but only to a certain altitude, at which restoring forces balance the displacing effect of the artificial heating.

[31] For clarity, the peak values in Figure 3 were cut off; the dotted line reaches a maximum value of 2.24 near 210 km, and a minimum of 0.45 at the heated spot of 380 km; the dashed line has a maximum of 2.25 at 210 km (unchanged from dotted line), and minimum of 0.42 at 380 km; the dash-dotted line has a maximum of 3.34 at 230 km, and a minimum of 0.37 at 380 km.

[32] The temperature of the system at the heated spot is evidently able to change much more rapidly than the density. This creates a temporary pressure imbalance which can drive this perturbation along the field line. Once the density perturbation has left the heated spot however, the heated spot is depleted, and pressure equilibrium is restored.

[33] The time evolution of the density perturbation at the heated spot is shown in Figure 4. The heater is turned on at t = 0 hours, and off at t = 5 hours. The density response is clearly seen. In this simulation, after nearly an hour of heating, the electrons reach their quasi-steady depletion state, with very little further depletion with continued heating. When the heat source is removed, the

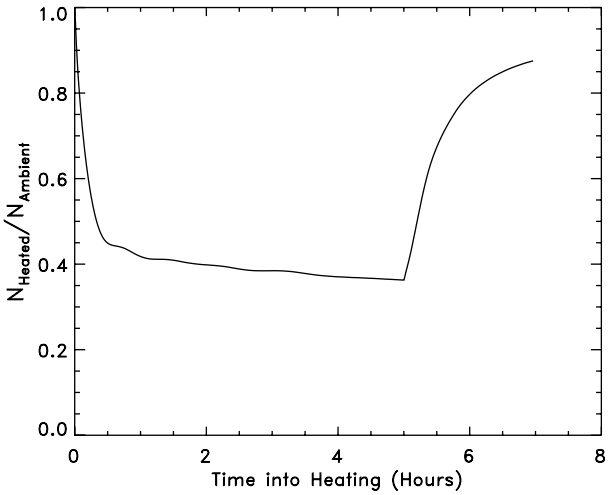

Figure 4. Density perturbation at the heated spot during artificial heating. The normalized density perturbation is on the vertical axis, and the horizontal axis is the time after heating began. Artificial heating ends at t = 5 hours. Heating parameters for these data are q = 5000 K/s and z_0 = 380 km.

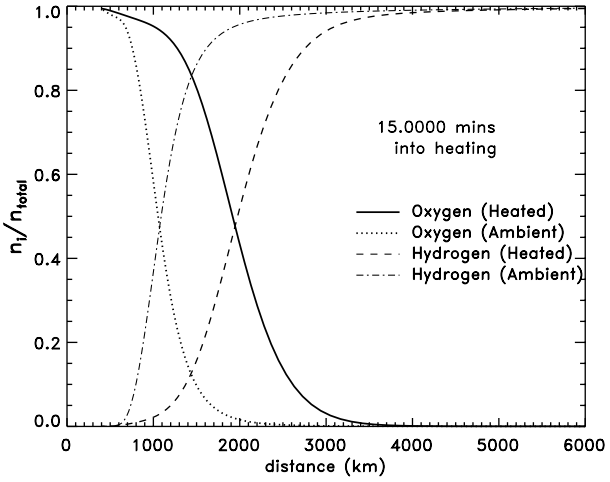

Figure 5. Changes in ion composition above the heated region during artificial heating. The vertical axis is the fraction of the total ion number density that is a single species, with solid and dotted lines representing O^+ and dashed and dash-dotted lines representing H^+, under both heated and ambient conditions. This plot represents the system after 15 min of artificial heating. Heating parameters for these data are q = 5000 K/s and z_0 = 380 km.

electrons rapidly increase in density, returning to ambient values.

[34] It is not simply a decrease in electron density which occurs at the heated region; the ions are moving with those electrons, and the species do not move uniformly. Figure 5 shows how the ion fraction can change with altitude during a simulation. The heated spot is again at 380 km, so these changes occur well above the heated region. In fact, the affected area (approximately 1500–3000 km along the line) is the same area which experiences an enhancement in electron density, seen in Figure 3. Clearly the dominant ion at low altitudes, O^+, rises up quickly during heating to enhance the density at those higher altitudes, changing the ion composition of those altitudes, and increasing the effective mass of the ionosphere (as O^+ is 16 times more massive than H^+). This change in ion composition takes less than 15 min of continuous heating to develop, and so this effect is potentially verifiable in practice if a satellite passes over a region experiencing artificial heating.

[35] Figure 6 displays the force density profile of the system for the two dominant ions, O^+ and H^+, at 3 times during a typical simulation. Force density is simply the acceleration of the material times its mass density, and following its evolution is similar to tracking sound wave

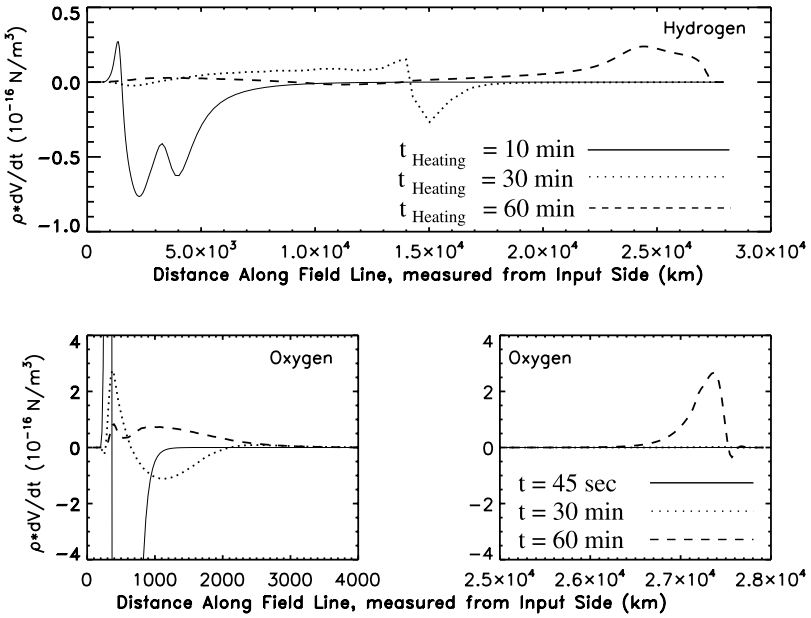

Figure 6. Propagation of force density perturbations during artificial heating for (top) H^+ only and (bottom) O^+ only. The vertical axis is the local mass density of the plasma times its local acceleration, with ambient force density subtracted to isolate perturbations from natural noise. The horizontal axis is the location on the field line, as measured along the line. The solid line in the top plot corresponds to 10 min after heating begins; the solid line in the bottom plots is 45 s after heating begins. In each, the dotted line is 30 min and the dashed line is 60 min after heating begins. Heating parameters for these data are q = 5000 K/s and z_0 = 380 km.

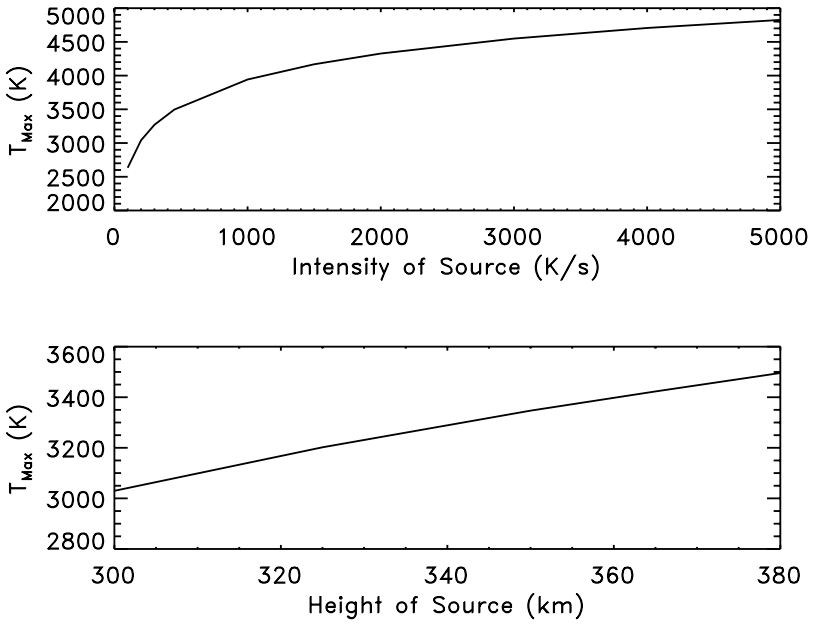

Figure 7. Maximum electron temperature attained by the heated region versus variations in heating parameters: (top) altitude of the heated region fixed at 380 km and (bottom) intensity fixed at 450 K/s. For comparison, the ambient temperature at this region was approximately 1250 K.

propagation in a medium [*Huba et al.*, 2000b]. This plot was produced by determining the force density in both heated and ambient data for each location and time, and subtracting the two in order to isolate the effects of heating only. This is necessary as the ambient plasma is not in equilibrium, because of diurnal variations, and natural density perturbations propagate through the plasma throughout the simulation. In this plot, negative values indicate material accelerating to the right of the plot, with the heated spot located at 380 km. The bottom plot is split into two in order to focus on the nonzero portions of the plot: There is very little O^+ at high altitudes, so the force density is thus very small.

[36] In the top plot of Figure 6, the solid line shows hydrogen ions are accelerating drastically away from the heated region 10 min after heating begins. The dotted line shows H^+ acceleration near the apex, 30 min into heating, with ions on the front of the pulse accelerating away from the heated spot, and ions on the tail end of the pulse accelerating back toward the heated region. The dashed line is 60 min into heating, showing that the pulse has traveled to the conjugate hemisphere in about an hour and has begun to dissipate.

[37] In the bottom plot of Figure 6, the solid line shows oxygen ions accelerating away from the heated region (located at 380 km) on both sides: positive acceleration on the left, and negative on the right. Note that the two peaks extend for over an order of magnitude above and below the bounds of the plot; most of the solid line is thus cut off in order to provide focus on the evolution of the pulse at later times. (For completeness the maximum value is 60, and the minimum is -210.) This drastic acceleration supports the explanation brought up in reference to Figures 3 and 5, that the O^+ ions are being forced away from the heated spot to locations above and below along the field line. Since the accelerations at these locations approach zero as the simulation continues, as seen in the dotted and dashed lines, the ion material must remain at those new locations under pressure equilibrium as long as the artificial heater remains in operation. The dashed line shows that at 60 min into heating, O^+ is similarly accelerated near the F_2 peak on the conjugate side as on the heated side, but to a much lesser extent than on the heated side.

4.2. Parametric Responses

[38] Below is a discussion of how various properties of the perturbation changed with the heating parameters: intensity q and location z_0.

[39] The value of z_0 during q variation was 380 km (heating directly at the F_2 layer), and q equaled 450 K/s (maximum intensity of the HAARP facility, before upgrades were made) during z_0 variation.

[40] First we compare how the magnitude of the perturbation at the heated spot varied with heating parameters. Figure 7 shows the maximum temperature

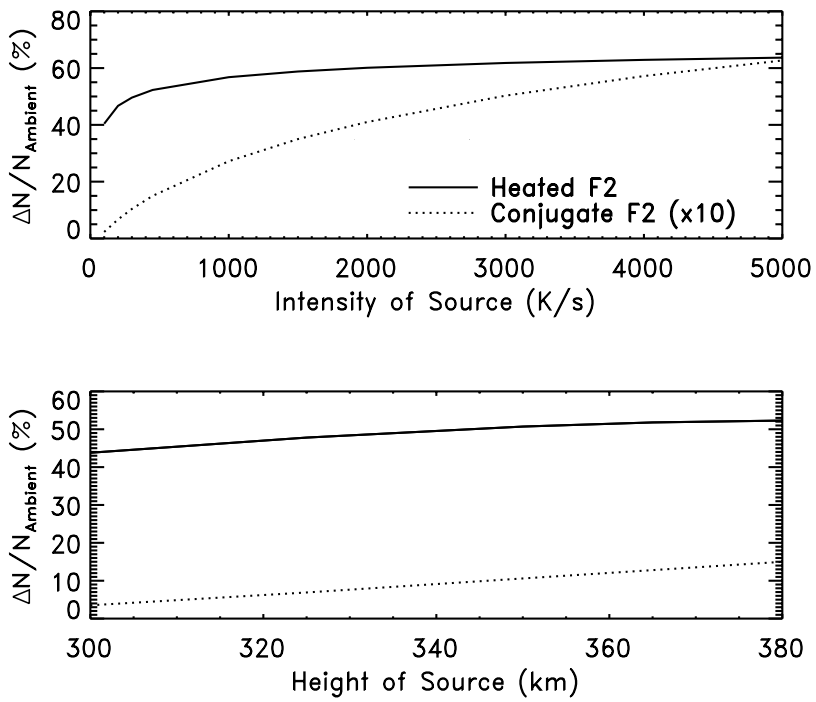

Figure 8. Maximum density depletion at the heated F_2 peak (solid line) and enhancements at the conjugate F_2 peak (dotted line) during artificial heating versus variations in heating parameters: (top) altitude of the heated region fixed at 380 km and (bottom) frame intensity fixed at 450 K/s. Note that the values from the conjugate side are multiplied by 10 in order to be visible on this scale.

attained by the heated spot versus q and z_0. As explained during the discussion of Figure 2, the maximum temperature is attained very quickly, on the timescale of less than a minute, and remained for the duration of heating. A nonlinear relationship emerges in the top plot, with a very nearly linear relationship in the bottom. Thus increasing the intensity of the source, after a somewhat linear region from 100 to 300 K/s, causes a saturation effect in the ionosphere, so it soon becomes clear that no matter how intense the source is, the heated region will not become any hotter. However, the altitude of the source is important, as heating directly on the F_2 layer (at 380 km in these simulations) causes the highest temperatures. Heating at a distance from this layer is not as efficient, and the temperature decreases linearly with that distance.

[41] Density perturbations, measured both at the heated F_2 layer, and at the conjugate F_2 peak (on the other side of the field line) are another important property of the perturbation. Figure 8 displays these results, with the measurements at the heated F_2 peak in solid lines, and the conjugate F_2 peak in dotted lines. The numbers here are presented in percentage change from ambient conditions. Note that the values on the conjugate side indicate increases from ambient density, and are multiplied by 10 so that they are visible on the same scale as the heated region data. The maximum depletion at the heated F_2 side was about 60%, in contrast to about 6% enhancement at the F_2 conjugate point.

[42] As in Figure 7, the perturbation properties here show a nonlinear saturation relationship with intensity but a linear relationship with altitude. Even the small perturbations occurring on the conjugate side match those on the heated side in behavior, if not exactly in slope.

[43] Figure 9 presents the characteristic heating and cooling times for each simulation. The characteristic time is the time taken for the electron density at the heated region to change by a factor of e; Figure 4 provides a good reference for this calculation. The heating time would then be the time taken to deplete the heated region by a factor of e from its value before heating (at $t = 0$ in Figure 4), and the cooling time is the time taken to increase in density from the most depleted value (at $t =$ 5 hours in Figure 4) by a factor of e. The measurable characteristic times are plotted in Figure 9, where the intensity relationship follows those in Figures 7 and 8, with a nonlinear saturation behavior.

[44] The propagation time of the perturbation in electron density to the conjugate F_2 peak was measured in

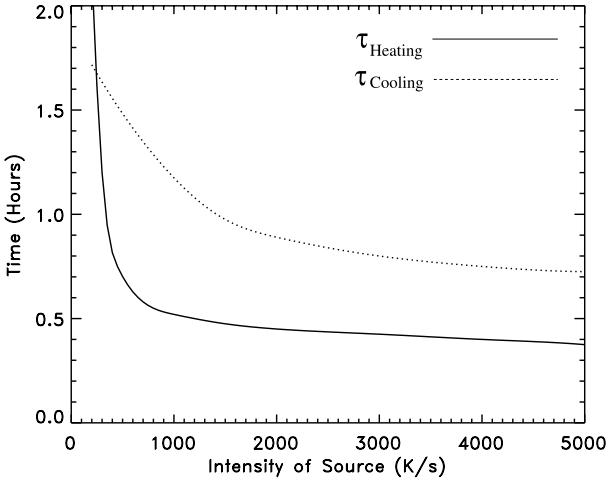

Figure 9. Characteristic heating (solid line) and cooling (dotted line) times versus variations in heating intensity; the altitude of the heated region was fixed at 380 km.

the code as well. The perturbation was observed to take 1–1.5 hours to reach the conjugate point from the onset of artificial F_2 peak heating. The range reflects a dependence on heating parameters to the travel time of the pulse: the time drops nonlinearly with increased energy pumping rate q, and linearly with increased altitude z_0, which indicates that a nonlinear propagation mechanism of the pressure pulse exists.

5. Discussion and Conclusions

[45] The primary conclusion that we can draw from the results of these simulations is that a perturbation in the plasma of the ionosphere, consisting of a pressure pulse, can be produced in our model as a result of strong artificial heating. This pulse is caused initially by the pressure imbalance at the heated spot, as the electrons there rapidly increase in temperature without a corresponding rapid decrease in density. This pulse propagates through the simulated plasma along the magnetic field line in both directions, toward lower and higher altitudes, passes the apex of the field line, and ultimately reaches the conjugate F_2 region. The pulse then dissipates in the heavier plasma at altitudes below the F_2 layer.

[46] Depending on the heating parameters, the perturbation in the simulations reaches the conjugate F_2 layer after 1–1.5 hours of continuous heating in these simulations. However, variations in pulse velocity cannot be accounted for by comparing the perturbation to the propagation of a sound pulse; some nonlinear mechanism must be present.

[47] After approximately 1 hour of modeled heating, the perturbed hemisphere settles into a new pressure equilibrium, forming a profile shown in Figure 3 (dash-dotted line), with enhancements in electron (and thus ion) density above and below the heated region, which itself experiences a depletion.

[48] All measurements of the perturbation (i.e., maximum temperature and minimum electron density of the heated region, electron density enhancement at the conjugate F_2 peak, characteristic heating and cooling times, and perturbation travel time) have a nonlinear saturation relationship with the intensity of the source, q. At lower intensities (100–300 K/s), this relationship is nearly linear, but quickly turns over and flattens out at higher intensities. It is clear that intensities higher than 5000 K/s would not cause appreciably larger perturbations using the constant heating scheme employed in these simulations.

[49] We find a linear relationship between the altitude of the heated spot (z_0) and these measurements, which has implications for the practical benefits of heating as close as possible to the F_2 layer. In our simulations, our imposed HF heating (see equation (2)) is presumed to occur via the resonant absorption effect, which has been studied by *Taran et al.* [1994] and *Gurevich et al.* [1996], for example. By this effect, strong plasma heating only occurs in a thin layer (5–10 km). This heating could then potentially drive the same pressure and density perturbations that we see in our simulations; however, in practice, this effect only occurs when heating directly on the F_2 peak (that is, when the heating frequency matches f_0F_2), and strong plasma heating does not occur efficiently when heating far below the F_2 peak. Our results show that if HF absorption could create strong plasma heating (equivalent to the resonant absorption effect) far from the F_2 peak, the resulting perturbations would be weaker proportional to the distance from the F_2 peak.

[50] An important consequence of our model showing that the perturbation traverses the entire field line, from one hemisphere to the other, is that the density along the entire line can possibly be affected by heating at a spot near one end of the line. This is the first step toward artificial duct formation. Further, if these density perturbations are confined to the heated field line, then a density gradient perpendicular to the line can form; enhanced density gradients cause higher index of refraction gradients, which form the boundaries of possible artificial ducts.

[51] ELF waves are channeled along a duct by total internal reflection off its boundaries, as long as the boundaries of the duct are significant enough—that is, if the density gradients are large enough. It is clear that the density perturbations in these simulations (see Figure 3) on the heated side of the field line are large; however the perturbations elsewhere are weak, amounting to only a

few percent along most of the field line, once the initial pressure pulse dissipates. Further work will be needed to create greater perturbations along the entire field line simultaneously, so that stronger uniform duct boundaries can be formed. We have not yet made estimates of the density gradients required to efficiently duct ELF waves, but work is in progress to explore this complex topic.

[52] Our results qualitatively agree with those from the previous 1-D studies by *Vas'kov et al.* [1992, 1993]. However, there are also distinctions associated with our different quantitative approaches. Our approach relies on changing the heating frequency in such a way that it matches the varying plasma frequency of the F_2 peak (a capacity which HAARP was designed to have), and on keeping the HF absorption constant. Vas'kov et al. assumed the heating frequency to be a constant while the heat source, caused by a model anomalous absorption, follows the modifications of the density profile and disappears after the F_2 peak is depleted. However, this would never happen in real HF-heating experiments because once the density depletes along the magnetic flux tube, the refracted HF wave would heat at nearby locations. We should note that there are quantitative differences between the results of the two studies which are due to different conditions modeled and different ionosphere-plasmasphere models employed.

[53] Finally, though the perturbations along the entire field line cannot be easily measured (as outlined in the introduction), these simulations have offered a method of detecting a signature of the transient perturbation with a single pass of a satellite during HF heating. Figure 5 shows that the ion composition drastically changes in a broad region along the magnetic field line above the heated spot, as the dominant ion changes from H^+ to O^+. If these perturbations are confined within the single magnetic field tube, then a satellite passing through this region, which is approximately 1500 km in length along the field line, should detect a drastic change in ion composition along its trajectory as it performs in situ measurements. The heated spot above HAARP is about 200 km wide, so a satellite would pass through this region in approximately 22 s. If these predictions are accurate, the satellite should detect a notable change in H^+ and O^+ density during those 22 s, indicating that perhaps O^+ has moved higher into the ionosphere.

6. Future Work

[54] This work is a first effort into understanding mechanisms that create artificial ducts in the ionosphere. Much can be done to further this effort.

[55] A future study will use SAMI2 to model the field lines above the HAARP site (62.4°N) to confirm the applicability of these results to higher latitudes. The current version of SAMI2 is a midlatitude model, and as such does not include certain high-latitude effects, such as particle precipitation and auroral electrojet activity. However, during quiet ionospheric conditions, such effects are absent, which happen to be the conditions most conducive to F layer heating. Thus the presence of a quiet ionosphere has already been implicitly assumed in this work. Therefore, in the context of F layer heating, SAMI2 should be physically applicable to higher latitudes. Preliminary runs show that modeled HF heating at high altitudes during quiet ionospheric conditions changes only the amplitude of the perturbations, because of the longer magnetic field line, and not the physical results.

[56] This work must also be performed in higher dimensions, as these were in essence 1-D simulations. The plasma was confined to the field line by assumption, so further study must be done to verify the behavior presented here.

[57] One of the higher-dimensional effects which must be examined is that of $\mathbf{E} \times \mathbf{B}$ drift of the field line during heating. If ionospheric convection causes the line to drift out of the irradiated region during heating, then that line is no longer experiencing heating. Neglecting drift is possibly quite significant, as this convection effect puts an upper limit on the time a single field line can be subject to heating. The convection timescale (in seconds) is

$$t_c = L/v_{cir} = 50\frac{L(\mathrm{km})}{E(\mathrm{mV/m})} \tag{5}$$

with L being the horizontal scale of the HF irradiated region in km, and v_{cir} being the convection velocity, which is proportional to the electric field strength E, in mV per meter. For example, consider a 100 km irradiated region (typical for heaters such as HAARP) in the midlatitudes, where E is of order 1 mV/m. This provides a t_c of order 5000 s, which is much longer than the 15–30 min taken to produce a significant perturbation in our work (see Figure 3). However, t_c should be lower at higher latitudes, where E is larger, so $\mathbf{E} \times \mathbf{B}$ drift could play a larger role at high latitudes.

[58] Limited 3-D ionospheric simulations have been performed in the past, though not with nearly the physical accuracy and detail which SAMI2 could provide. For example, simple 3-D computations have been performed using a cylindrically symmetrical model of duct formation in a homogeneous medium, including transverse thermal conductivity. Figure 10 shows how the plasma density depletion develops in time and space during these simulations. The first plot shows that at τ = 1 (in dimensionless units) only a slight perturbation in the electron density appears. Its amplitude increases as it propagates deep inside the media as illustrated by the

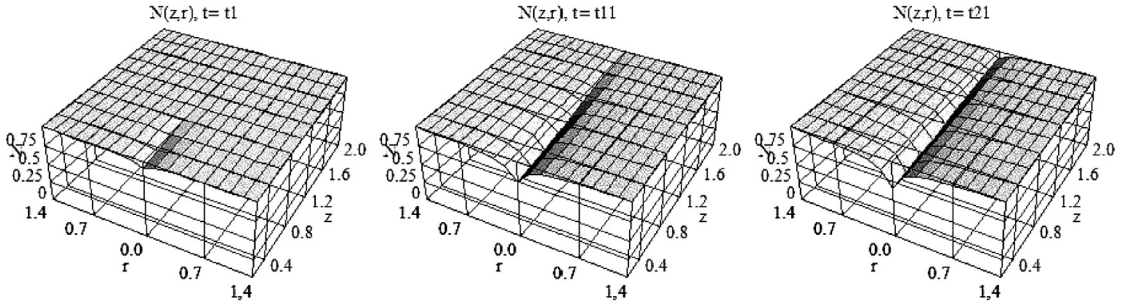

Figure 10. Temporal evolution of a plasma density depletion in the uniform ionosphere with cylindrical symmetry at (left) $t = 1$, in dimensionless units; (middle) $t = 11$; and (right) $t = 21$. Here z is along the field line, while r is perpendicular to the line. The vertical axis is plasma density, in units normalized to the ambient values.

three plots in Figure 10 (taken at $\tau = 1$, 11 and 21 in dimensionless time).

[59] This duct formation principle should be applied to fully 3-D models as well for a more comprehensive understanding of how the perturbations transverse to the field line develop. This understanding is critical, as ducts are produced when perturbations of the electron density, due to the HF heating, spread perpendicular to the magnetic field line, leading to ELF refraction and ducting. The 1-D model presented here does not allow us to study the plasma distribution across the cross section of a field line; however, simple 3-D models, such as the one depicted in Figure 10, can model 3-D density perturbations excited by HF heating in uniform plasma. SAMI2 does have 2-D capabilities, with many 1-D field lines stacked above one another, however we chose to restrict our work to one field line as we sought to explore the possibility of duct formation without undue initial complexity. A fully 3-D global version of the model exists as well, called SAMI3, which can be used in the future to study the more complex effects present in higher dimensions.

[60] The density perturbations must also be enhanced so that they are more uniform across the field line if the duct boundaries are to reliably reflect ELF waves. It is possible that modulated heating of ionosphere could produce this effect: it has been informally observed in this model that if the heater is turned on and off repeatedly, multiple pulses can be produced which follow one another down the field line. Since the perturbation pulse carries a larger density perturbation than the steady state (see Figure 3), it would seem logical to fill the field line with pulses which follow one another in rapid succession. Figure 11 displays density profiles during an initial test of this concept. As in Figure 3, the maximum and minimum values have been cut off for practical purposes (peak values are similar to those in Figure 3, as discussed in section 4.1).

[61] In this simulation, the artificial heater was repeatedly turned on and off at regular intervals (21 min on, and 21 min off) to explore the possibility of creating multiple pulses. Two such pulses in the plasma are labeled in the plot: pulse "A" is generated when the heater turns on during the plotted cycle, while pulse "B" was generated during the previous cycle. In the solid

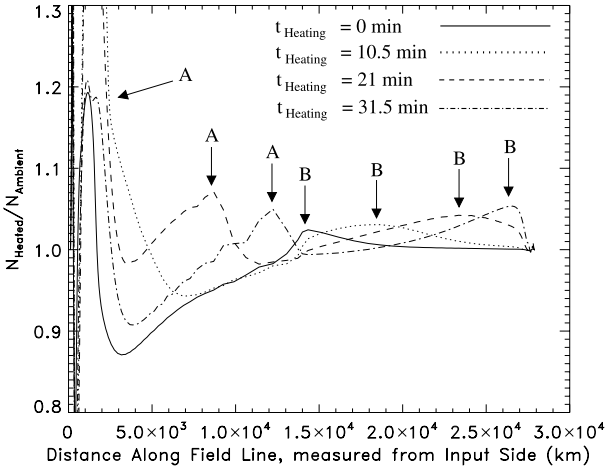

Figure 11. Density perturbation profile during a simulation with periodic artificial heating. In this run, a heating cycle of 21 min of heating followed by 21 min of cooling was used. The solid line corresponds to the end of a cycle; the dotted line is 10.5 min after heating begins, halfway through a heating phase; the dashed line is 21 min into the cycle, just as the heater turns off; and the dash-dotted line shows conditions 31.5 min into the cycle, after 10.5 min of cooling. Arrows label two separate pulses propagating simultaneously within the plasma. Heating parameters for these data are $q = 450$ K/s and $z_0 = 380$ km.

line, pulse B is visible near the apex of the line. The dotted line represents the system ¼ of a cycle later, when the density perturbation has grown greatly near the heated region, but a new pulse has yet to emerge. Meanwhile, the pulse from the previous phase (pulse B) has continued to move toward the conjugate region, but has broadened significantly, with a peak near 18,000 km. The dashed line is halfway through the heating cycle, right before the heater shuts off; a well-defined pulse (pulse A) is evident on the heated side, near 8,000 km, and the pulse from the previous cycle (B) has continued to move and broaden, with a peak now near 24,000 km. Finally, the dash-dotted line shows the new pulse (A) peaking at approximately 12,000 km, and the old pulse (B) has narrowed again as it stops near the conjugate F_2 peak. Thus two pulses are discernible simultaneously throughout the 42 min cycle. This suggests that the efficiency of artificial duct formation could be improved by pulsed heating.

[62] **Acknowledgments.** This work uses the SAMI2 ionosphere model written and developed by the Naval Research Laboratory, and our research is sponsored by the High-frequency Active Auroral Research Program (HAARP) and the Office of Naval Research (ONR). This research was also supported by NSF grant ATM-0317261.

References

Barr, R., and P. Stubbe (1993), ELF harmonic radiation from the Tromsø heating facility, *Geophys. Res. Lett.*, *20*(20), 2243–2246.

Duncan, L. M., J. P. Sheerin, and R. A. Benke (1988), Observation of ionospheric cavities generated by high-power radio waves, *Phys. Rev. Lett.*, *61*(2), 239–242.

Ferraro, A. J., H. S. Lee, T. W. Collins, M. Baker, D. Werner, F. M. Zain, and P. J. Li (1989), Measurements of extremely low frequency signals from modulation of the polar electrojet above Fairbanks, Alaska, *IEEE Trans. Antennas Propag.*, *37*, 802–805.

Gurevich, A. V., and G. M. Milikh (1997), Artificial airglow due to modifications of the ionosphere by powerful radio waves, *J. Geophys. Res.*, *102*(A1), 389–394.

Gurevich, A. V., A. V. Lukyanov, and K. P. Zybin (1996), Anomalous absorption of powerful radio waves on the striations developed during ionospheric modification, *Phys. Lett. A*, *211*, 363–372.

Hedin, A. E., et al. (1991), Revised global model of the thermosphere winds using satellite and ground-based observations, *J. Geophys. Res.*, *96*(A5), 7657–7688.

Helliwell, R. A. (1974), Controlled VLF wave injection experiments in the magnetosphere, *Space Sci. Rev.*, *15*, 781–802.

Huba, J. D., G. Joyce, and J. A. Fedder (2000a), SAMI2 is another model of the ionosphere (SAMI2): A new low-latitude ionosphere model, *J. Geophys. Res.*, *105*(A10), 23,035–23,053.

Huba, J. D., G. Joyce, and J. A. Fedder (2000b), Ion sound waves in the topside low altitude ionosphere, *Geophys. Res. Lett.*, *27*(19), 3181–3185.

Inan, U. S., M. Golkowsky, D. L. Carpenter, N. Reddell, R. C. Moore, T. F. Bell, E. Paschal, P. Kossey, E. Kennedy, and S. Z. Meth (2004), Multi-hop whistler-mode ELF/VLF signals and triggered emissions excited by the HAARP HF heater, *Geophys. Res. Lett.*, *31*, L24805, doi:10.1029/2004GL021647.

Papadopoulos, K., T. Wallace, M. McCarrick, G. M. Milikh, and X. Yang (2003), On the efficiency of ELF/VLF generation using HF heating of the auroral electrojet, *Plasma Phys. Rep.*, *29*, 561–565.

Papadopoulos, K., T. Wallace, G. Milikh, W. Peter, and M. McCarrick (2005), The magnetic response of the ionosphere to pulsed HF heating, *Geophys. Res. Lett.*, *32*, L13101, doi:10.1029/2005GL023185.

Picone, J. M., A. E. Hedin, D. P. Drob, and A. C. Aikin (2002), NRLMSISE-00 empirical model of the atmosphere: Statistical comparisons and scientific issues, *J. Geophys. Res.*, *107*(A12), 1468, doi:10.1029/2002JA009430.

Taran, V. I., L. P. Goncharenko, V. K. Bogovskiy, and V. N. Lysenko (1994), Modifications of electron temperature and concentration in ionospheric *F* region due to impact of high-power radio waves, *Geomagn. Aeron.*, *33*(6), 791–795.

Vas'kov, V. V., Y. S. Dimant, N. A. Ryabova, V. V. Klimenko, and L. M. Duncan (1992), Thermal disturbances of the magnetospheric plasma upon resonant heating of the *F* layer of the ionosphere by the field of a powerful radio wave, *Geomagn. Aeron.*, *32*(5), 698–706.

Vas'kov, V. V., Y. S. Dimant, and N. A. Ryabova (1993), Magnetospheric plasma thermal perturbations induced by resonant heating of the ionospheric *F*-region by high-power radio waves, *Adv. Space Res.*, *13*(10), 1025–1033.

Y. Dimant, Center for Space Physics, Boston University, Boston, MA 02215, USA. (dimant@bu.edu)

G. M. Milikh, K. Papadopoulos, and R. P. Perrine, Department of Astronomy, University of Maryland, College Park, MD 20742, USA. (milikh@astro.umd.edu; kp@astro.umd.edu; perrine@astro.umd.edu)

J. D. Huba, Plasma Physics Division, Naval Research Laboratory, Washington, DC 20375, USA. (huba@ppd.nrl.navy.mil)

G. Joyce and M. Swisdak, Icarus Research, Inc., Bethesda, MD 20892, USA. (joyce@ppd.nrl.navy.mil; swisdak@ppd.nrl.navy.mil)